

Microscopic Insights for Beyond Room-Temperature Ferromagnetism in Ni doped Two-Dimensional Fe_5GeTe_2

Sukanya Ghosh, Soheil Ershadrad and Biplab Sanyal*

Department of Physics and Astronomy, Uppsala University, Box-516, 75120, Uppsala, Sweden

E-mail: *biplab.sanyal@physics.uu.se

Abstract. Enhancement of Curie temperature (T_C) of two-dimensional (2D) magnets is immensely desirable for room temperature spintronic applications. Fe_5GeTe_2 is an exceptional van der Waals metallic ferromagnet due to its tunable physical properties and relatively higher T_C than other 2D magnets. Using density functional theory combined with dynamical mean field theory and Monte Carlo simulations, we show that the T_C of Fe_5GeTe_2 monolayer can increase well-above room temperature by substitutional doping with Ni. It is found that two specific sublattices (Fe1 and Fe4) are the first and second most energetically preferred occupation sites for Ni. T_C of $\text{Fe}_{5-\delta}\text{Ni}_\delta\text{GeTe}_2$ increases up to ~ 400 K at $\delta \sim 20\%$. Exchange interactions between particular Fe5-Fe4 pairs play a dominating role in tuning the transition temperature, influenced by doping-induced structural distortions. Finally, we highlight the effect of dynamical electron correlation in site-specific electronic structure and quasi-particle mass of Fe- d orbitals with varying Ni doping.

1. Introduction

Atomically thin, layered quasi-two-dimensional (2D) van der Waals (vdW) crystals exhibit exceptional physical properties [1,2]. Regarding 2D magnets, however, according to the Mermin-Wagner theorem, an intrinsic long-range magnetic order can not exist in the isotropic 2D limit because strong thermal fluctuations prohibit continuous symmetries to break spontaneously [3]. The presence of weak magnetic anisotropy is sufficient to open up a sizable gap in the magnon spectra, causing long-range magnetic order to persist in materials with dimension $D \leq 2$ at a finite temperature.

Among the newly discovered vdW magnetic materials [1, 4–12], metallic Fe_nGeTe_2 ($n = 3, 4, 5$) [13–17] systems, commonly referred to as FGT are quite special. Ferromagnetism close to room temperature increases their demand for spintronic applications. This can be further enhanced by applying pressure [18, 19], gating [20, 21], carrier doping [22, 23], ion intercalation [24], etc. It has also been found that substitutional doping of Fe_5GeTe_2 with cobalt increases the magnetic ordering temperature to ~ 360 K influencing the magnetic ground state, interlayer stacking and magnetic textures [23, 25–27]. A recent study by Chen et al. has reported an enhancement of ferromagnetism in bulk $\text{Fe}_{5-\delta}\text{GeTe}_2$ up to 478 K with Ni doping [16]. The authors showed that Ni doping triggers structural modifications, influences saturation magnetization, and affects T_C . However, a detailed description of microscopic mechanisms determining the observed trend for T_C in $\text{Fe}_{5-\delta}\text{Ni}_\delta\text{GeTe}_2$ is still lacking. Especially, the exact nature of magnetic interactions governing T_C should be unveiled. How the tuning of exchange interactions caused by structural modifications in $\text{Fe}_{5-\delta}\text{Ni}_\delta\text{GeTe}_2$ determines T_C , demands a thorough investigation.

In this Letter, performing first-principles calculations, we investigate the rationals responsible for the enhancement of T_C well above room temperature by substitutional doping with Ni in Fe_5GeTe_2 monolayer. We find out which particular Fe sites are more prone to host Ni dopant. Our study explains how the tuning of exchange interactions between certain Fe pairs, caused by structural modifications, plays the dominating role to increase T_C up to a certain doping. Reduction in T_C for higher doping is caused by the replacement of magnetic Fe atom by nonmagnetic Ni, however, the dominating exchange still remains ferromagnetic, as observed in experiment [16], but in contrast with a recent DFT study [28].

A $\sqrt{3} \times \sqrt{3}$ cell of Fe_5GeTe_2 monolayer in UDU (Up-Down-Up) configuration of Fe atoms is considered in this study, where two (Fe1U) and one (Fe1D) Fe atoms are situated directly above and below Ge, respectively [13, 29–31]. We investigate magnetic and electronic properties of the energetically favored configurations, determined by comparing the total energies of $\text{Fe}_{5-\delta}\text{Ni}_\delta\text{GeTe}_2$ monolayers varying the position(s) of Ni dopant(s).

Our results show that the in-plane lattice parameter a remains almost unaltered compared to the undoped system till $\delta = 27\%$, and starts to reduce when $\delta > 30\%$, see Fig. 1(a). However, the thickness d of the monolayer increases with doping up to

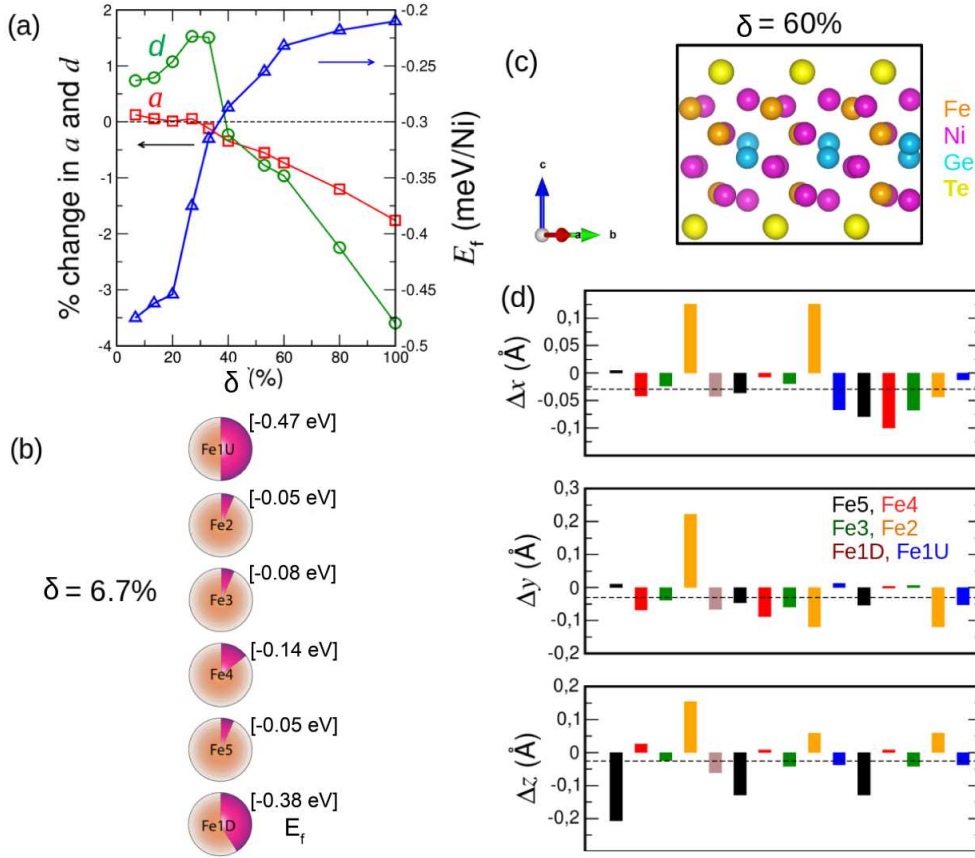


Figure 1. (a) Percentage change of in-plane lattice parameter a (red squares), thickness d (green circles) and formation energy E_f (blue triangles), respectively, for $\text{Fe}_{5-\delta}\text{Ni}_\delta\text{GeTe}_2$ monolayer with Ni doping (δ). (b) Schematics showing formation energy (E_f) of $\text{Fe}_{5-X}\text{Ni}_X\text{GeTe}_2$ for different Ni occupation site. Purple area indicates the tendency of a Fe sublattice to get substituted with Ni, numbers show E_f for different Fe sites at $\delta = 6.7\%$. (c) Side view of $\text{Fe}_{5-\delta}\text{Ni}_\delta\text{GeTe}_2$ at $\delta = 60\%$. The height of histograms shows rumpling of each Fe/Ni atom along x , y and z directions present at the unit cell of $\delta = 60\%$ wrt the undoped monolayer, horizontal dashed line shows the average rumpling.

$\delta = 20\%$ but reduces for $\delta \geq 40\%$ as shown in Fig. 1(a). Substitutional doping of Ni in Fe_5GeTe_2 monolayer becomes energetically less favored with increase in δ . This is evident in Fig. 1(a) (blue triangles) where the formation energy E_f per Ni dopant is observed to increase with δ . It is also worth noting that during the substitutional doping, the replacement of Fe1 species with Ni is energetically more favored than other Fe sites. Between $\delta = 6.7\%$ (Fe1U) and 20% (Fe1U+Fe1U+Fe1D) only Fe1 sublattice gets substituted by Ni. After Fe1, the next energetically favored occupation site for Ni dopant is Fe4. There is a significant increase in E_f between $\delta = 20\%$ and 27% , when one of the Fe4 atoms gets substituted together with Fe1U and Fe1D species. The presence of Ni causes an excess of electrons (Fig S1), which might cause the lowering of E_f . For $\delta \geq 33\%$, Fe atoms belonging to other Fe sublattices (Fe2, Fe5 and Fe3) start to get

substituted along with Fe1 and Fe4. Fig. 1(b) shows how E_f varies when Ni substitutes different Fe sublattices at $\delta = 6.7\%$.

Structural distortion or rumpling (along x , y and z directions) in the monolayer increases with Ni-doping (Fig. S1). Fig. 1(c) shows the side view when $\delta = 60\%$. The height of the histograms in Fig. 1(d) shows the difference in x , y and z coordinates between Fe or Ni atoms present in 60% Ni-doped and undoped systems for each (Ni/Fe) site of $\sqrt{3} \times \sqrt{3}$ cell. $\delta = 60\%$ causes significant rumpling of the atoms present at the sites of Fe5 (along z) and Fe2 sublattices. Negative value of average rumpling (dashed horizontal line) supports the compression of cell parameters (both a and d) with Ni doping, as we see in Fig. 1(a). It should be noted that Ref. 16 also finds a reduction in layer thickness with an increase in Ni doping. Apart from substitutional doping, Ni can occupy any vacant site of $\sqrt{3} \times \sqrt{3}$ cell of $\text{Fe}_{5-\delta}\text{GeTe}_2$, including vdW gap between different layers, such scenario can be present in experiments performed at a finite temperature [16].

In our previous study, we showed that the inclusion of dynamical electron

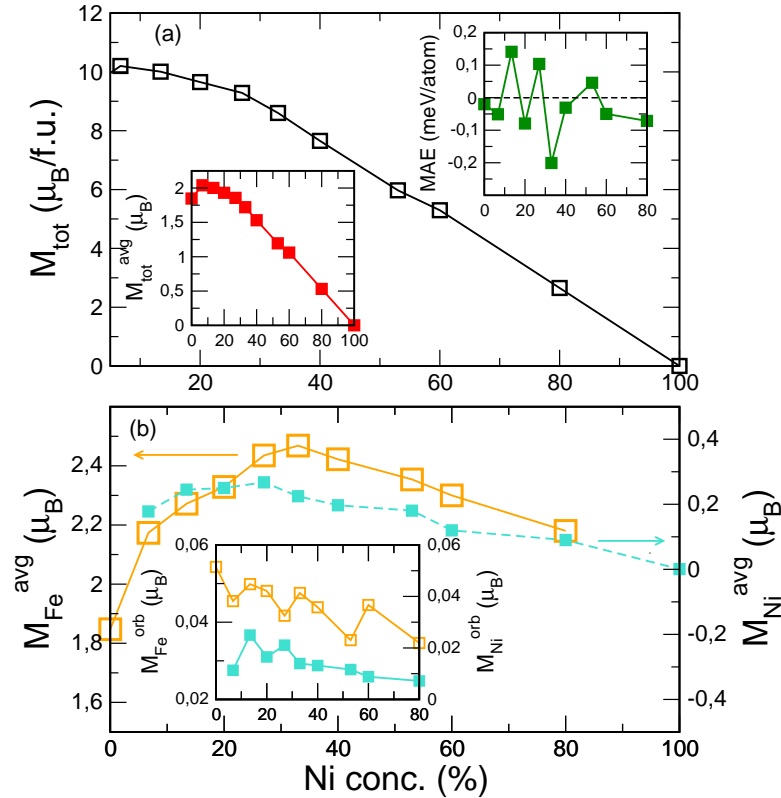


Figure 2. (a) Total magnetic moment (M_{tot}) of $\text{Fe}_{5-\delta}\text{Ni}_\delta\text{GeTe}_2$ monolayer as a function of doping concentration δ . Insets with red and green squares show the average of total magnetic moment $M_{\text{tot}}^{\text{avg}}$ and variation of magnetic anisotropy energy (MAE) as a function of δ , respectively. (b) Variation of average magnetic moment of Fe ($M_{\text{Fe}}^{\text{avg}}$, orange squares) and Ni ($M_{\text{Ni}}^{\text{avg}}$, cyan squares) atoms plotted with δ . Inset shows average orbital moment $M_{\text{orb}}^{\text{avg}}$ for Fe (orange) and Ni (cyan) for different δ .

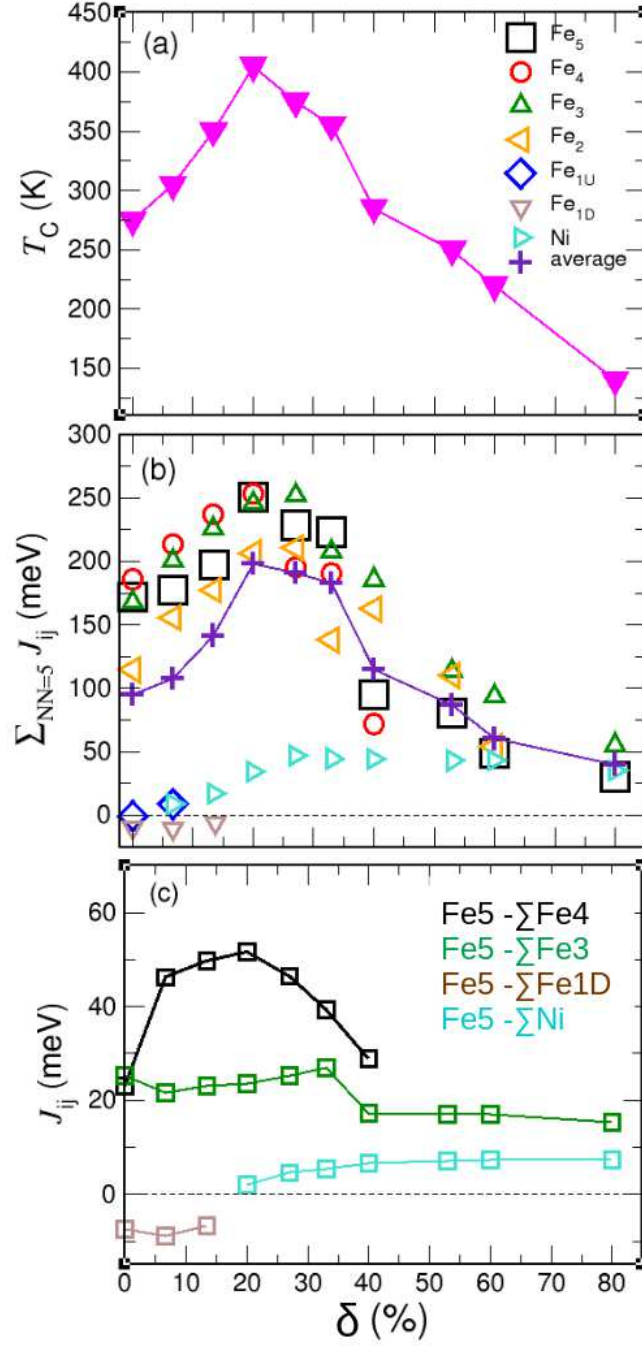


Figure 3. (a) Variation of $\sum_{NN=5} J_{ij}$ with δ for each Fe sublattice. $\sum_{NN=5} J_{ij}$ is sum of isotropic symmetric exchange interactions J_{ij} over the first five nearest neighbors. (b) Variation of T_C with δ . (c) J_{ij} interactions between $i = \text{Fe}_5$ and $j = \sum \text{Fe}_4$, $\sum \text{Fe}_3$, $\sum \text{Fe}_{1D}$ and $\sum \text{Ni}$ with δ .

correlation effect is an appropriate approach to determine the magnetic moment, exchange interactions and T_C of the Fe_nGeTe_2 systems, compared to the standard GGA and GGA+U methods [14]. Therefore, we perform charge self-consistent dynamical

mean-field theory (DFT+DMFT) calculations as implemented in the FP-LMTO code RSPt [32, 33] to investigate the magnetic and electronic properties of $\text{Fe}_{5-\delta}\text{Ni}_\delta\text{GeTe}_2$ monolayer. The computational details are mentioned in SI.

Doping with Ni influences the magnetism of $\text{Fe}_{5-\delta}\text{Ni}_\delta\text{GeTe}_2$ monolayer. The total spin moment M_{tot} reduces as a function of doping (δ). Fig. 2(a) shows that M_{tot} decreases from $10 \mu_B$ to $0 \mu_B$ from $\delta = 0\%$ to 100% . These results are in good agreement with the saturation magnetic moment of bulk $\text{Fe}_{5-\delta}\text{Ni}_\delta\text{GeTe}_2$. [29] It is interesting to note that the direction of easy axis or magnetic anisotropy energy, MAE ($= E_{\parallel} - E_{\perp}$) oscillates between in-plane and out-of-plane directions with δ . However, for most of the doped systems, the easy axis lies in the xy -plane, see green squares presented as an inset in Fig. 2(a), which is in agreement with experiment [16]. The strength of MAE for $\text{Fe}_{5-\delta}\text{Ni}_\delta\text{GeTe}_2$ monolayers is much weaker than pristine Fe_3GeTe_2 and Fe_4GeTe_2 monolayers [14, 21]. The trend observed for MAE at lower δ values can be correlated with the value of orbital moments obtained for different directions of spin axis [34], see Table S2. It is worth noting that the switching of the easy axis is observed in $\text{Fe}_{5-\delta}\text{GeTe}_2$ with Co doping and electrical gating [23, 35]. Experiments report switching of easy axis for bulk Fe_5GeTe_2 depending on the Fe concentration [29, 36]. The average spin moment of Fe atoms first increases with doping, becomes maximum at $\delta = 33\%$, then reduces, see Fig. 2(b). Similar to Ref. 16, our calculations also find that Ni dopants carry negligible spin moment (cyan squares in Fig. 2(b)) and are not responsible for the origin or tuning of ferromagnetism. The average orbital moment $M_{\text{orb}}^{\text{avg}}$ of Fe remains between 0.05 and 0.04 till $\delta=80\%$, see inset of Fig. 2(b). The orbital moment of Ni falls in the range of 0.01-0.02 and reduces for higher δ .

We calculate the isotropic symmetric (J_{ij}) and antisymmetric (D_{ij}) exchange interactions present in $\text{Fe}_{5-\delta}\text{Ni}_\delta\text{GeTe}_2$ monolayer varying δ . Incorporating J_{ij} , D_{ij} and MAE in the Heisenberg Spin-Hamiltonian (Eq. S4), T_C is computed performing Monte Carlo simulations. Fig. 3(a) shows there is a monotonic increase of T_C up to $\delta = 20\%$, then it reduces. Qualitative trend of T_C vs. δ plotted in Fig. 3 agrees well with experimental reports on bulk $\text{Fe}_{5-\delta}\text{Ni}_\delta\text{GeTe}_2$ [16]. The critical δ value at which T_C of the monolayer becomes maximum, is not exactly the same as observed in the experiment. This slight discrepancy happens because in experiments, during the doping process, Ni can be placed at any vacant position present in the bulk without replacing Fe, enhancing ferromagnetism and hence T_C . However, the rationale behind such trend of T_C in $\text{Fe}_{5-\delta}\text{Ni}_\delta\text{GeTe}_2$ is not addressed in the previous study.

Comparing the strength of different magnetic interactions we expect J_{ij} couplings must play the dominating role to determine T_C , in agreement with our study on pristine FGT systems [14]. In order to investigate the tuning of J_{ij} with δ , we plot the J_{ij} values summed over the first five nearest neighbors (NNs) for different i th Fe sublattices, see Fig. 3(b). We consider NN up to 5, because the J_{ij} interactions decay significantly beyond that, see Figs.S4-S7. Most of the Fe sublattices show dominating ferromagnetic (FM) J_{ij} interactions while Fe1D and Fe1U show antiferromagnetic (AFM) interactions, till $\delta = 13.4\%$.

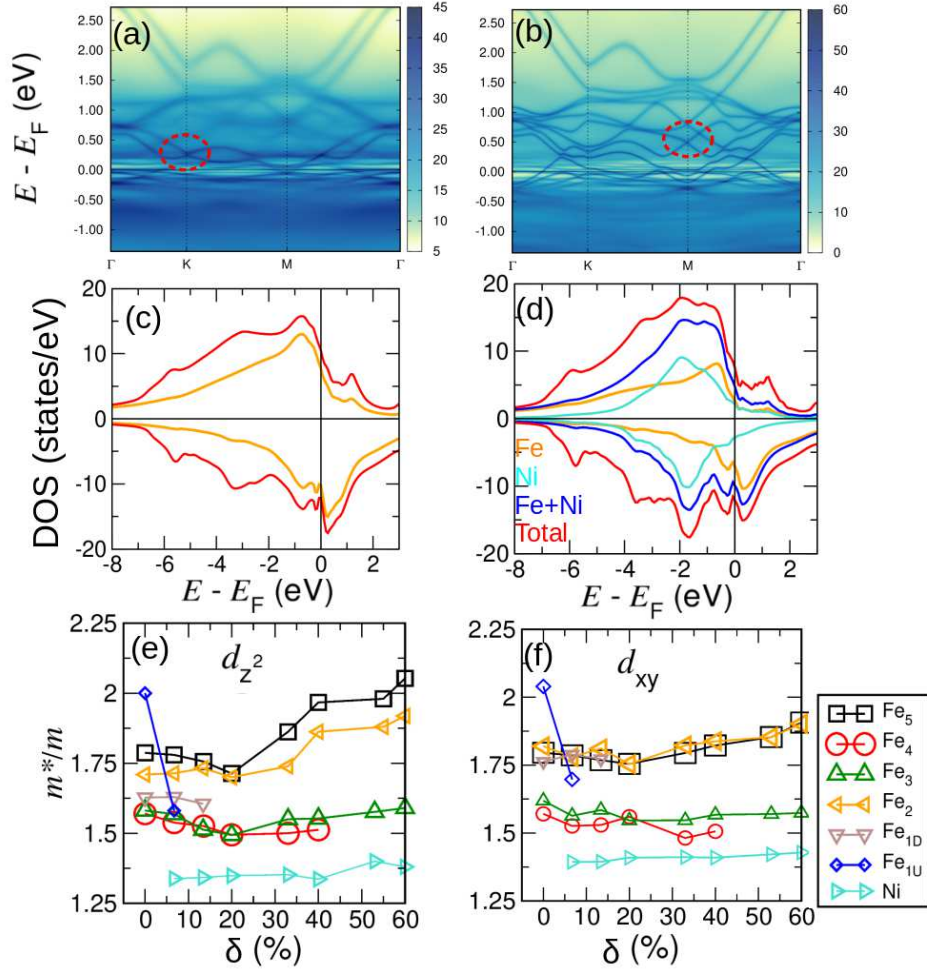


Figure 4. Spectral function plots for $\delta =$ (a) 0% and (b) 40%. The Dirac-cone-type features present at the high-symmetry points K (a) and M (b) are highlighted by the red circles. (c) and (d) DOS at $\delta = 0\%$ and 40%, respectively. Effective mass, m^*/m for (e) Fe- d_z^2 and (f) d_{xy} for different Fe sublattices and Ni with δ . These results are obtained at $T = 155$ K.

The $\sum_{NN=5} J_{ij}$ term for Fe5, Fe4, Fe3 and Fe2 first increases with δ , becomes maximum for $\delta = 20\%$, then reduces for higher concentration. $\sum_{NN=5} J_{ij}$ is plotted for each Fe species present in the $\sqrt{3} \times \sqrt{3}$ cell. A monotonic increase of $\sum_{NN=5} J_{ij}$ for each Fe sublattice (except Fe1U and Fe1D) is observed up to $\delta = 20\%$. This happens because till $\delta = 20\%$, except Fe1, the number of Fe sublattices present in the unit cell is 3. For $\delta > 20\%$ the Fe atoms belonging to Fe4 sublattice start to get substituted in addition with Fe1U and Fe1D, as we see in Fig. 1(d). The replacement of magnetic Fe causes sharp reduction in $\sum_{NN=5} J_{ij}$ of Fe4 for $\delta > 20\%$. After 40% all three Fe4 atoms get substituted with Ni, see red circles in Fig. 3(a). The gradual replacement of different Fe sublattices with Ni causes rapid lowering in $\sum_{NN=5} J_{ij}$ for $\delta \geq 33\%$. In addition to possessing negligible magnetic moment (Fig. 2), Ni dopants have negligible contribution to the J_{ij} interactions. The magnitude of $\sum_{NN=5} J_{ij}$ for Ni

is ~ 10 times smaller than the Fe sublattices for $\delta \leq 20\%$. As the number of Ni atoms present in $\text{Fe}_{5-\delta}\text{Ni}_\delta\text{GeTe}_2$ increases with δ , $\sum_{NN=5} J_{ij}$ for Ni becomes comparable with Fe for $\delta \geq 60\%$. For $i=\text{Ni}$, non-zero exchange couplings exist when $j=\text{Fe}$, otherwise, interactions between Ni themselves is rather weak. The violet symbols show the average variation of $\sum_{NN=5} J_{ij}$ with Ni doping, which increases from 0% to 20% and then reduces. The same investigation has been made for D_{ij} interactions as well. For a given δ , the magnitude of $\sum_{NN=5} D_{ij}$ for any i th Fe species is ~ 10 times smaller than $\sum_{NN=5} J_{ij}$ (Fig S9).

Further analysis of J_{ij} couplings among individual Fe pairs reveals that the interactions between Fe5 and Fe4 play the dominating role. Fig 3(c) shows J_{ij} interactions when $i = \text{Fe5}$ and j th species are considered to be the nearest neighbors of Fe5, i.e., Fe4, Fe3, Fe1D and Ni. We find, among these neighbors, exchange coupling between Fe5- \sum Fe4 plays dominating role to control or tune the T_C . The J_{ij} interaction between Fe5 and Fe4 increases with δ and then reduces for $\delta \geq 27\%$. The increase of J_{54} up to $\delta = 20\%$ occurs due to the following reasons: i) reduction of Fe5-Fe4 bond length with δ (Fig. S2), ii) among the first five NNs of Fe5, three of them are Fe4 species with the strongest FM coupling. Therefore, $J_{54} = (J_{54_1} + J_{54_2} + J_{54_3})$ for $\delta \leq 20\%$. The reduction in J_{54} for $\delta > 20\%$ occurs due to the gradual replacement of Fe4 with Ni, causing a decrease in the number of Fe4 belonging to the first five NN of Fe5, see Fig. S3 for details. No particular trend is observed for J_{53} (green squares), up to $\delta = 60\%$. J_{ij} exchange interactions between Fe5 and Fe1D is AFM (brown squares), and replacement of Fe1D with Ni triggers FM exchange coupling (cyan squares). Comparing different J_{5j} interactions we see J_{54} follows the similar trend as $\sum_{NN=5} J_{5j}$ (black squares) and average of $\sum_{NN=5} J_{ij}$ (purple symbols) in Fig. 3(b). Therefore, J_{54} has major influence on T_C , especially for $\delta \leq 20\%$. From Fig. 3(a) - (c) we can establish the fact that T_C not only depends on the strength of J_{ij} but also on the nearest neighbor (NN) distance or effective coordination number.

Now we discuss how Ni doping modifies the electronic structure. Figs. 4(a) and (b) show the spectral function $A(k, \omega)$ for $\delta = 0\%$ and 40% . The main differences observed in $A(k, \omega)$ at these two values of δ are: i) at the high-symmetry point K , there is presence of Dirac-cone-type feature for $\delta = 0\%$, which disappears at $\delta = 40\%$, ii) at M , Dirac-cone is observed for $\delta = 40\%$ which is not present for the undoped monolayer. The density of states (DOS) plots for $\delta = 0\%$ and 40% are plotted in Figs. 4(c) and (d), respectively, (see Fig. S16 for details). The intensity of DOS projected on Fe reduces with Ni doping. The Fe states have dominating contribution close to E_F , maximum intensity of Ni states arises away from E_F . Similar to other FGT systems, the admixture of localized and itinerant electrons exists in Fe_5GeTe_2 as well [14, 37]. The effective mass $(m^*/m)_{l\sigma}$ provides the quantitative measurements of electronic correlation [38] (see Eq. S7). Both qualitative and quantitative trends of m^*/m with δ remain almost unaltered for different Fe- d states, see Figs. 4(e)-(f) and Fig.S17. m^*/m of Fe reduces between $\delta = 0\%$ and 20% , then increases for $\delta > 20\%$, especially for Fe5 and Fe2. $(m^*/m)_{l\sigma}$ of Fe5, Fe2 are larger than for Fe3, Fe4. This implies the d electrons belong to Fe5 and Fe2 sublattices

are more correlated than Fe3 and Fe4. Similar to $\text{Fe}_{5-\delta}\text{GeTe}_2$, site-dependence of Fe sublattices is present in Fe_3GeTe_2 as well [39]. Interestingly, the effective mass of Ni-*d* is lower than Fe-*d*, signifying the Ni-*d* states are less correlated or more delocalized than Fe-*d*.

In summary, we investigate the effect of Ni doping on the structural, electronic, and magnetic properties of $\sqrt{3} \times \sqrt{3}$ $\text{Fe}_{5-\delta}\text{Ni}_\delta\text{GeTe}_2$ monolayer using DFT+DMFT and Monte Carlo simulations. Our results show that T_C of the monolayer increases up to ~ 400 K by substitutional doping with Ni. The variation in T_C of $\text{Fe}_{5-\delta}\text{Ni}_\delta\text{GeTe}_2$ monolayer with doping is in good agreement with a recent experimental report on bulk $\text{Fe}_{5-\delta}\text{Ni}_\delta\text{GeTe}_2$. Moreover, we identify the dominant exchange interactions responsible for the observed trend in T_C . Our results show the structural modifications caused by the Ni dopant, thereby modifying the nearest neighbor distances and effective coordination numbers, which affect the dominating exchange couplings. Our study also shows how Ni-doping influences site-dependent spectral features and effective masses arising from electron correlation.

Acknowledgments

B.S. and S.G. acknowledge a postdoctoral grant from Carl Tryggers Stiftelse (CTS 20:378). B. S. acknowledges financial support from Swedish Research Council (grant no. 2022-04309). The computations were enabled in project SNIC 2022/3-30 by resources provided by the Swedish National Infrastructure for Computing (SNIC) at NSC, PDC, and HPC2N partially funded by the Swedish Research Council (Grant No. 2018-05973). B.S. acknowledges allocation of supercomputing hours by PRACE DECI-17 project ‘Q2Dtopomat’ in Eagle supercomputer in Poland and EuroHPC resources in Karolina supercomputer in Czech Republic and LUMI supercomputer in Finland.

2. References

- [1] Gibertini M, Koperski M, Morpurgo A F and Novoselov K S 2019 *Nat. Nanotech.* **14** 408–419
- [2] Gong C and Zhang X 2019 *Science* **363** eaav4450
- [3] Mermin N D and Wagner H 1966 *Phys. Rev. Lett.* **17**(22) 1133–1136
- [4] Burch K S, Mandrus D and Park J G 2018 *Nature* **563**(7729) 47–52
- [5] Zollner K, Gmitra M and Fabian J 2020 *Phys. Rev. Lett.* **125**(19) 196402
- [6] Zhu W, Song C, Han L, Guo T, Bai H and Pan F 2022 *Nat. Commun.* **13**(1) 6428
- [7] Verzhbitskiy I A, Kurebayashi H, Cheng H, Zhou J, Khan S, Feng Y P and Eda G 2020 *Nat. Electron.* **3**(8) 460–465
- [8] Lee I, Utermohlen F G, Weber D, Hwang K, Zhang C, van Tol J, Goldberger J E, Trivedi N and Hammel P C 2020 *Phys. Rev. Lett.* **124**(1) 017201
- [9] Wang C, Gao Y, Lv H, Xu X and Xiao D 2020 *Phys. Rev. Lett.* **125**(24) 247201
- [10] Jiang S, Li L, Wang Z, Mak K F and Shan J 2018 *Nat. Nanotech.* **13**(7) 549–553
- [11] Ghosh S, Stojić N and Binggeli N 2021 *Nanoscale* **13**(20) 9391–9401
- [12] Ghosh S, Stojić N and Binggeli N 2019 *Physica B: Condensed Matter* **570** 166–171
- [13] Ershadrad S, Ghosh S, Wang D, Kvashnin Y and Sanyal B 2022 *J. Phys. Chem. Lett.* **13** 4877–4883

- [14] Ghosh S, Ershadrad S, Borisov V and Sanyal B 2022 Unraveling effects of electron correlation in two-dimensional Fe_nGeTe_2 ($n=3, 4, 5$) by dynamical mean field theory
- [15] Seo J, Kim D Y, An E S, Kim K, Kim G Y, Hwang S Y, Kim D W, Jang B G, Kim H, Eom G, Seo S Y, Stania R, Muntwiler M, Lee J, Watanabe K, Taniguchi T, Jo Y J, Lee J, Min B I, Jo M H, Yeom H W, Choi S Y, Shim J H and Kim J S 2020 *Sci. Adv.* **6** 8912
- [16] Chen X, Shao Y T, Chen R, Susarla S, Hogan T, He Y, Zhang H, Wang S, Yao J, Ercius P, Muller D A, Ramesh R and Birgeneau R J 2022 *Phys. Rev. Lett.* **128**(21) 217203
- [17] Zhao B, Ngaloy R, Ghosh S, Ershadrad S, Gupta R, Ali K, Hoque A M, Karpiak B, Khokhriakov D, Polley C, Thiagarajan B, Kalaboukhov A, Svedlindh P, Sanyal B and Dash S P 2023 *Advanced Materials* 2209113
- [18] Bhoi D, Gouchi J, Hiraoka N, Zhang Y, Ogita N, Hasegawa T, Kitagawa K, Takagi H, Kim K H and Uwatoko Y 2021 *Phys. Rev. Lett.* **127**(21) 217203
- [19] Hu X, Zhao Y, Shen X, Krashennnikov A V and Chen Z 2020 *ACS Appl. Mater. Interfaces* **12**(23) 26367–26373
- [20] Deng Y, Yu Y, Song Y, Zhang J, Wang N Z, Sun Z, Yi Y, Wu Y Z, Wu S, Zhu J, Wang J, Chen X H and Zhang Y 2018 *Nature* **563**(7729) 94–99
- [21] Kim D, Lee C, Jang B G, Kim K and Shim J H 2021 *Sci. Rep.* **11**(1) 17567
- [22] Weber D, Trout A H, McComb D W and Goldberger J E 2019 *Nano Lett.* **19**(8) 5031–5035
- [23] May A F, Du M H, Cooper V R and McGuire M A 2020 *Phys. Rev. Mater.* **4** 074008
- [24] Wang N, Tang H, Shi M, Zhang H, Zhuo W, Liu D, Meng F, Ma L, Ying J, Zou L, Sun Z and Chen X 2019 *J. Am. Chem. Soc.* **141**(43) 17166–17173
- [25] Zhang H, Shao Y T, Chen R, Chen X, Susarla S, Raftrey D, Reichenadter J T, Caretta L, Huang X, Settineri N S, Chen Z, Zhou J, Bourret-Courchesne E, Ercius P, Yao J, Fischer P, Neaton J B, Muller D A, Birgeneau R J and Ramesh R 2022 *Phys. Rev. Mater.* **6**(4) 044403
- [26] Zhang H, Raftrey D, Chan Y T, Shao Y T, Chen R, Chen X, Huang X, Reichenadter J T, Dong K, Susarla S, Caretta L, Chen Z, Yao J, Fischer P, Neaton J B, Wu W, Muller D A, Birgeneau R J and Ramesh R 2022 *Sci. Adv.* **8** eabm7103
- [27] Tian C, Pan F, Xu S, Ai K, Xia T and Cheng P 2020 *Appl. Phys. Lett.* **116**(20) 202402
- [28] Hu X, Yao D X and Cao K 2022 *Phys. Rev. B* **106** 224423
- [29] Zhang H, Chen R, Zhai K, Chen X, Caretta L, Huang X, Chopdekar R V, Cao J, Sun J, Yao J, Birgeneau R and Ramesh R 2020 *Phys. Rev. B* **102**(6) 064417
- [30] May A F, Ovchinnikov D, Zheng Q, Hermann R, Calder S, Huang B, Fei Z, Liu Y, Xu X and McGuire M A 2019 *ACS nano* **13** 4436–4442
- [31] May A F, Bridges C A and McGuire M A 2019 *Phys. Rev. Mater.* **3** 104401
- [32] Grånäs O, Di Marco I, Thunström P, Nordström L, Eriksson O, Björkman T and Wills J 2012 *Comput. Mater. Sci.* **55** 295–302 ISSN 0927-0256
- [33] Wills J, Eriksson O, Alouani M and Price D 2000 *Full-Potential LMTO Total Energy and Force Calculations* (Berlin, Heidelberg: Springer Berlin Heidelberg)
- [34] Bruno P 1989 *Phys. Rev. B* **39**(1) 865–868
- [35] Tang M, Huang J, Qin F, Zhai K, Ideue T, Li Z, Meng F, Nie A, Wu L, Bi X, Zhang C, Zhou L, Chen P, Qiu C, Tang P, Zhang H, Wan X, Wang L, Liu Z, Tian Y and Iwasa Y 2022 *Nat. Elect.*
- [36] May A F *et al.* 2019 *ACS nano* **13** 4436–4442
- [37] Zhao M, Chen B B, Xi Y, Zhao Y, Xu H, Zhang H, Cheng N, Feng H, Zhuang J, Pan F, Xu X, Hao W, Li W, Zhou S, Dou S X and Du Y 2021 *Nano Lett.* **21**(14) 6117–6123
- [38] Ramšak A, Horsch P and Fulde P 1992 *Phys. Rev. B* **46**(21) 14305–14308
- [39] Kim T J, Ryee S and Han M J 2022 *npj Comput. Mater.* **8**(1) 245